Expanded View Figures

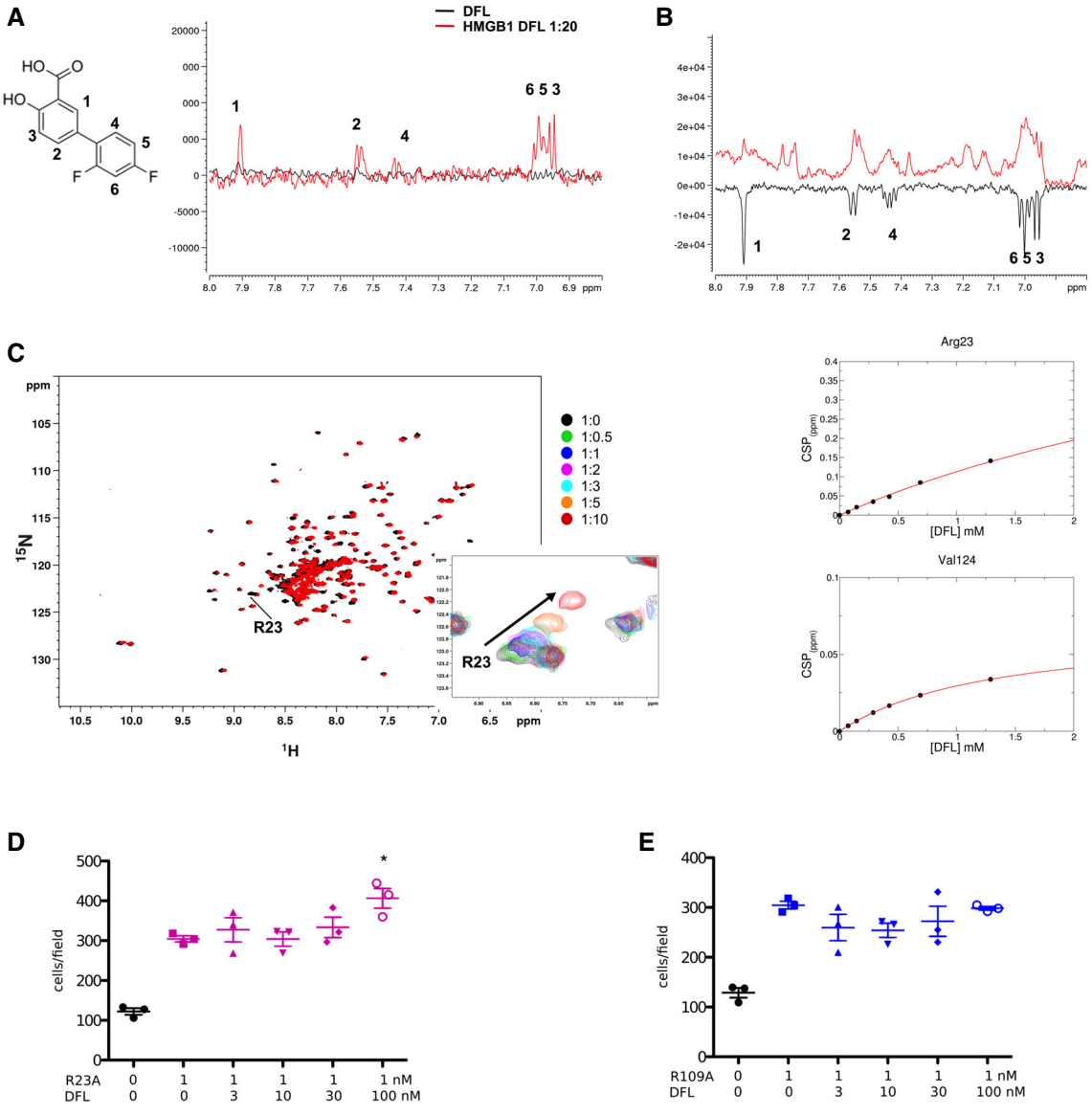

Figure EV1. Binding of DFL to HMGB1 assessed by NMR and chemotaxis experiments on R23A and R109A HMGB1 mutants.

A Saturation transfer difference (STD) results obtained for 1 mM DFL alone (black line) and with 0.05 mM HMGB1 (red line) in 20 mM phosphate buffer, 150 mM NaCl, 1 mM DTT pH 7.3 (on resonance: 0 ppm; saturation time: 3 s). STD signals with different intensities are observed for all protons in the presence of HMGB1, indicating that DFL directly binds to HMGB1. The numbered peaks correspond to proton resonance assignments.

B WaterLOGSY spectra obtained for 1 mM DFL alone (black line) and in complex with 0.05 mM HMGB1 (red line). All DFL protons display signals inversion, indicating binding to HMGB1.

C Superimposition of the ^{1}H-^{15}N HSQC spectra of HMGB1 (~0.1 mM, pH 7.3, phosphate buffer, 1 mM DTT) without (black) and with 10-fold excess of DFL (red). Inset: selected region of the superimposition of ^{1}H-^{15}N HSQC spectra of HMGB1 during the titration with DFL (0.5, 1, 2, 3, 5, and 10 equivalents) showing the displacement of the peak associated to R23 along the titration. On the right: weighted average of R23 and V124 amide ^{1}H and ^{15}N chemical shift changes in the presence of increasing concentration of DFL. Nonlinear curve fitting yields K_d = 2.8 ± 1.4 mM.

D, E The R23A (D) and R109A (E) HMGB1 mutants have chemotactic activity but are not inhibited by DFL. Data points with average ± standard deviation (avg ± SD; n = 3, each point represents a biological replicate) in one representative experiment (of two experiments performed in different days). Statistics: one-way ANOVA ($P < 0.0001$), followed by Dunnett's post-tests. *$P < 0.05$ relative to no DFL addition. The difference in migration toward R109A HMGB1 in the presence of increasing concentrations of DFL is statistically non-significant (one-way ANOVA plus post-tests).

Source data are available online for this figure.

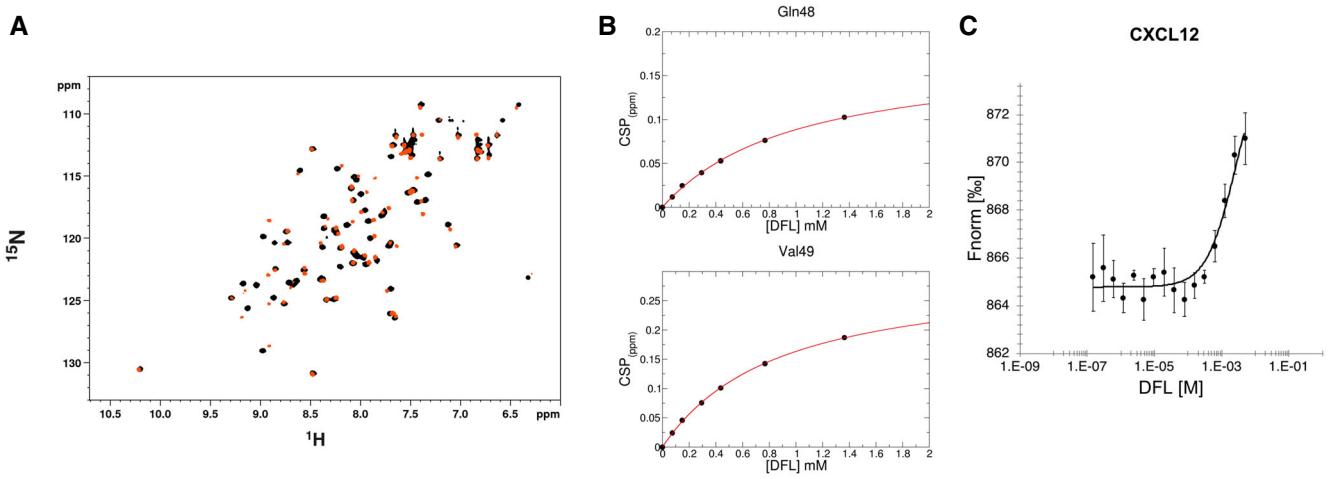

Figure EV2. Binding of DFL to CXCL12 assessed by NMR and MST.

A Superposition of ^{1}H-^{15}N HSQC spectra of CXCL12 (~0.1 mM, pH 6, phosphate buffer) without (black) and with 10-fold excess of DFL (orange).

B Weighted average of Q48 and V49 amide ^{1}H and ^{15}N chemical shift changes in the presence of increasing concentration of DFL. Nonlinear curve fitting yields K_d = 802 ± 102 μM.

C Dose–response curve of CXCL12-DFL interaction followed by MST. DFL concentrations ranged from 5 mM to 153 nM on 50 nM labeled 6His-CXCL12. The K_d is 2.6 ± 1.2 mM (n = 3, error bars correspond to SD). Saturation of the curve could not be reached because of solubility issues for DFL stock solutions > 10 mM. (Fnorm = normalized fluorescence).

Source data are available online for this figure.

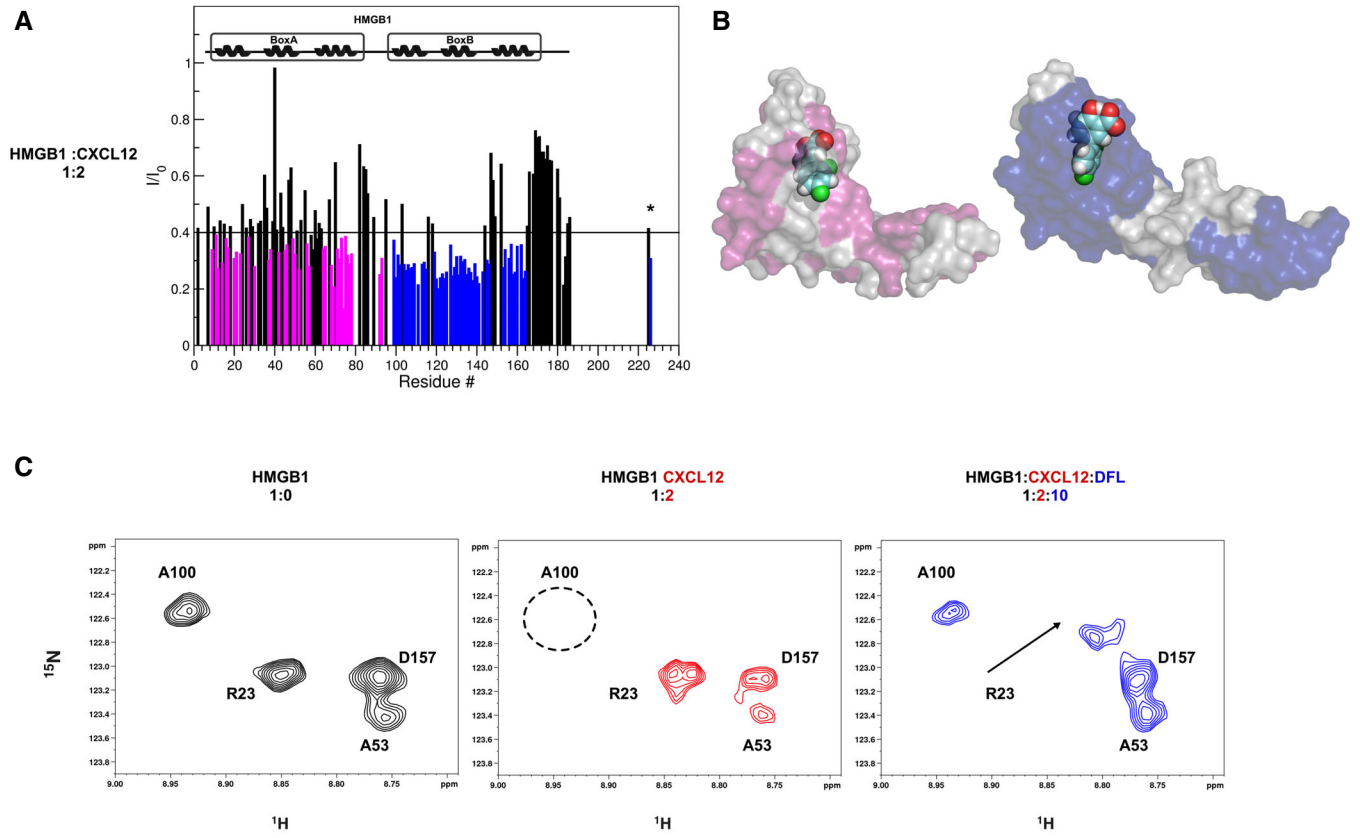

Figure EV3. DFL and CXCL12 binding surfaces on HMGB1 partially coincide and details of DFL effects on NMR spectra of the HMGB1/CXCL12 heterocomplex.

A Histograms showing the I/I_0 peak intensity ratio of HMGB1 amides (~0.1 mM, pH 6, phosphate buffer, 1 mM DTT) with and without twofold excess of CXCL12 (bottom). I_o and I are peak intensities in free and bound HMGB1, respectively. Residues showing significant decrease of I/I_0 ratio (I/I_0 ratio < avg) upon CXCL12 binding are represented with magenta (Box A) and blue (Box B) histograms. α-helices are schematically represented on the top of the histogram.

B Surface representations of Box A-DFL and Box B-DFL molecular models are reported where the residues showing significant decrease of I/I_0 ratio (I/I_0 ratio < avg) upon CXCL12 binding are mapped in magenta and blue, respectively.

C Selected region of ^{1}H-^{15}N-HSQC spectra of HMGB1 (~0.1 mM, pH 6, phosphate buffer, 1 mM DTT) without (black), with twofold excess of CXCL12 (red) and 10-fold excess of DFL (blue). In the presence of CXCL12, the HMGB1 spectrum undergoes line broadening and some peaks (e.g., A100 in Box B, black dotted circle) disappear, indicating complex formation. The A100 peak reappears in the ^{1}H-^{15}N-HSQC spectrum of HMGB1 upon addition of DFL, whereas the sites involved in binding to DFL are shifted (e.g., R23).

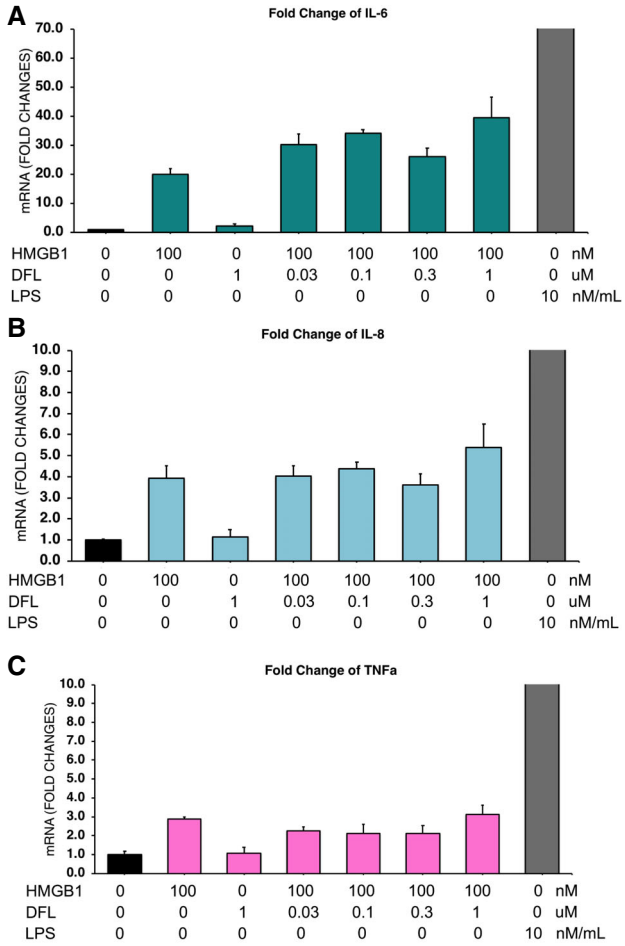

Figure EV4. DFL does not affect the cytokine-inducing activities of disulfide HMGB1 on human macrophages.

A–C Human macrophages were obtained as described [6] and activated or not for 3 h with 3 μg/ml disulfide HMGB1 (~100 nM) or 10 ng/ml LPS, in the presence of the indicated concentrations of DFL. The bars represent the avg ± SD (n = 3 biological replicates). In all cases, the mRNA levels (of *IL6*, *IL8*, *TNF*) in cells exposed to disulfide HMGB1 (ds-HMGB1) are not different in the presence of increasing concentrations of DFL (one-way ANOVA plus post-tests). This experiment was performed twice with macrophages generated from different donors.

Source data are available online for this figure.

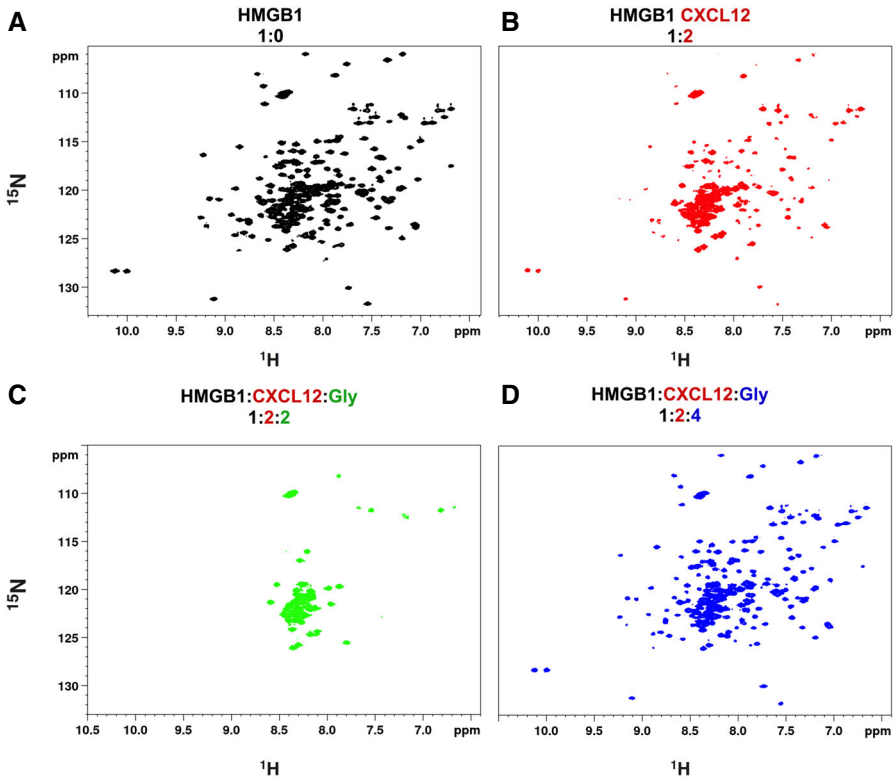

Figure EV5. Effects of Glycyrrhizin on the HMGB1/CXCL12 heterocomplex.

A–D ^{1}H-^{15}N HSQC HMGB1 (~0.1 mM) spectrum (A) without (black), (B) with a twofold excess of CXCL12 (red), (C) upon addition of twofold (green), and (D) fourfold excess of Glycyrrhizin (Glyc) (blue).